Russian Physics Journal, Vol. 56, No. 7, December, 2013 (Russian Original No. 7, July, 2013)

OPTICS AND SPECTROSCOPY

LASER SENSING OF THE ATMOSPHERE AND UPPER LAYER OF THE OCEAN BY AN AIRBORN AND SHIPBORNE LIDARS

V. S. Shamanaev UDC 551.5

General principles and approaches are described for the functioning of the multipurpose automated lidar complex "Atmaril" and results are presented of atmospheric-optical and hydro-optical measurements by a lidar mounted on board an aircraft and a scientific-research vessel.

Keywords: laser sensing of sea water and cloudiness, airborne and shipborne lidars.

INTRODUCTION

Recently, interest has grown in the use of airborne and shipborne lidars for sensing of the atmosphere and the upper layer of the ocean. The main advantage in their use over stationary lidars consists in the possibility of surveying large areas over a relatively short time. This makes it possible to obtain the spatial, that is to say, horizontal and vertical, distribution of light-scattering properties of the investigated medium with the aim of extracting data on the structure and dynamics of the atmospheric boundary layer above dry land, water areas, and in coastal regions; on the height of the mixing layer, the spatial distribution of the marine and continental aerosol, and also on such parameters of the ocean water column as the depth of the photophoretic layer, the distribution with depth of water turbidity, hydrosol concentration, phytoplankton, dissolved organic matter, yellow substance, chromophores, other pollutants, etc. [1–7].

The present paper describes the general principles and approaches to the functioning of a multipurpose automated lidar complex for sensing of the atmosphere and upper layer of the ocean from onboard an aircraft or scientific research vessel, developed on the basis of an analysis of the general requirements on the parameters of single-frequency airborne and shipborne lidars dictated by the specifics of the problem to be solved, including the use of tilted mirrors to vary the angle of the emitted radiation. Results are presented of atmospheric sensing to detect local sources of aerosol pollution. Results are also presented of sensing of the upper layer of the ocean to measure the bottom depth in shallow water and the optical characteristics of underwater hydrosol layers.

1. GENERAL REQUIREMENTS ON THE PARAMETERS OF AIRBORNE AND SHIPBORNE LIDARS

Airborne and shipborne lidars should have not too large weight and size and not too high energy requirements. The transmitter-receiver apertures also have limitations on their output dimensions, i.e., hatches in the airplane fuselage or ship hull. Specialization of the lidar is also of significance. A special-purpose lidar is compact and can be housed in a remote (suspended or other autonomous) container. The solution of a wide spectrum of research problems envisages a significantly more compact lidar and the possibility of its modification. The system for recording return signals of airborne and shipborne lidars should have maximum possible rapid response. The signal accumulation regime (photon

---

V. E. Zuev Institute of Atmospheric Optics, Siberian Branch of the Russian Academy of Sciences, Tomsk, Russia, e-mail: shvs@iao.ru. Translated from Izvestiya Vysshikh Uchebnykh Zavedenii, Fizika, No. 7, pp. 82–89, July, 2013. Original article submitted April 15, 2013.

counting) here is inefficient due to motion of the carrier platform. The dynamic range of the recorded signal should be large, especially for sensing clouds and sea water, where attenuation decrements of the signal are high.

Data interpretation requires that we solve the lidar sensing equation. In the single-scattering approximation it has the form

$$F(x) = F_0 A \frac{\varepsilon(x)}{x^2} \Delta x \,, \tag{1}$$

where $F(x)$ is the power of the signal received from a distance x, A is the instrumental constant, Δx is the spatial extent (or length) of the laser pulse, $\varepsilon(x)$ is the attenuation (scattering) coefficient of laser radiation in the investigated medium. To solve the inverse problem in the single-scattering approximation, the length of the laser pulse Δx should be such that the following condition is fulfilled:

$$\int_0^{\Delta x} \varepsilon(x)\Delta x << 1 \,. \tag{2}$$

Hence, in the case of sensing of clouds with scattering coefficient up to 50 km^{-1} (0.05 m^{-1}) [8] it follows that the pulse duration should not exceed 5–10 ns. For sensing of moderately turbid water with $\varepsilon \le 0.3$ m^{-1} [9] it is desirable to have a pulse with duration around 1 ns.

In the choice of wavelength of laser radiation, the solution can go in one of two ways. For the majority of practical problems of single-frequency sensing of clouds, wavelengths in the range from the near UV to the near IR do not have decisive importance, one way or the other. It is only important not to fall into any strong selective absorption line, for example, 694.38 nm for water vapor. The other application is sensing the water column, which has a blue-green range of enhanced transparency due to the physics of the molecular absorption of water [9]. The wavelength of the laser is chosen in this range. Here the maximum sensing depth of the lidar can vary from 9 to 50 m [3] depending on water turbidity and the presence of impurities and suspensions. If the aim is to sense phytoplankton chlorophyll, which occupies a thickness of several tens of meters, then, even using the both approaches, the result obtained is roughly the same. In the first, green radiation penetrates into water relatively deeply and excites fluorescence over the entire penetration depth, but it is not very intense. Its wavelength is centered at 680 nm, i.e., this is red radiation, having a large absorption coefficient in water. Thus, the fluorescence from deep water levels does not reach the water surface, and all of the fluorescence signal is formed in the first few meters of the subsurface water layer. In the second approach, it is better to sense the water column with ultraviolet radiation, for example, the third harmonic of the garnet laser at 355 nm. In this case, the intensity of the fluorescence return signal is substantially higher. However, the penetration depth of UV radiation in water is extremely small – it can be measured in units of centimeters. That means that all of the return signal is formed in the very upper layer of the ocean. In this case, there is no special reason to increase the power of sensing radiation since in this situation the return signal is formed nonlinearly. On this basis, for a multipurpose lidar intended for sensing both the sea water and the cloudy atmosphere, the most acceptable wavelength is in the blue-green range. From the standpoint of technical development, as a rule, this is second-harmonic radiation of a garnet laser (532 nm). Such lasers have been available for a long time and are quite reliable and relatively simple to use. “Hot” neon ion lasers with $\lambda = 540.1$ nm are also used. Copper-vapor lasers also have a suitable wavelength, but are unconvenient for use on board an aircraft. The use of nonlinear parametric wavelength converters for the majority of sensing problems is either uneconomical or simply inefficient.

One more important point – the high optical density of objects under study – leads to very rapid loss of coherence of laser radiation as it penetrates through them. Thus, in lidars intended for such use it is possible to analyze only the energy and polarization characteristics of the signals without complicating their design with heterodyne systems. This lowers the cost of the device many times due to its simpler design.

The parameters of the “Atmaril” lidar [8], intended for solving a wide class of problems of both a scientific and an applied nature on monitoring of the environment, are listed in Table 1.

TABLE 1. Parameters of the "Atmaril" Lidar

TRANSMITTER	
Wavelength of laser radiation, nm	532
Polarization	linear
Radiation pulse energy, mJ	50
Laser pulse duration, ns	8
RECEIVER	
Field of view, mrad	2–12
Diameter of Keplerian receiver telescope, cm	15
Temporal resolution of the photomultiplier, ns	15
Quantization step of the ADC, ns	10
Bit size of the ADC	8
Minimum atmospheric sensing range, m	50
Maximum atmospheric sensing range, m	10
Cloud detection range, km	up to 5
Cloud sensing depth, m	50…300
Sea water sensing depth (depending on its turbidity), m	up to 20
Measurable bottom depth, m	up to 35
Overall dimensions, m	1.0 × 1.2 × 0.7
Weight, kg	250
Power supply, kVA	up to 2

The lidar was mounted on board an AN-30 aircraft-laboratory and on board the *Academician Keldysh* Scientific Research Vessel.

2. USE OF TILTED MIRRORS

Lidars frequently employ mirror scanning systems. In some problems the need arises to sense an object of interest through an intermediate mirror that changes the direction of the optical axis, e.g., when sensing the lower boundary of clouds with an airborne lidar through an illuminator or when sensing the sea surface and the upper water layer with a shipborne lidar through a ship cabin window. As was shown in [10], in this case an additional phase difference Δ arises between the orthogonal components of the polarization as well as a difference in the reflection coefficients $\rho_\perp$ and ρ_{II} , both of which depend on the mirror material and the incident angle φ, which leads to distortions in the Stokes vectors of both the transmitted signal and the received signal. Thus, the sensing radiation after reflection from the mirror has $S_{01} = \widehat{M}S_0$, where $\widehat{M}$ is the reflection matrix. According to [11] the matrix $\widehat{M}$ can be obtained from the matrices of a linear phase compensator with phase delay Δ and a partial polarizer with relative amplitude attenuation $\tan\psi = \rho_\perp/\rho_{II}$ for the perpendicular and parallel components of the electric field vector $\boldsymbol{E}$:

$$\widehat{M} = \begin{pmatrix} 1 & -\cos 2\psi & 0 & 0 \\ -\cos 2\psi & 1 & 0 & 0 \\ 0 & 0 & \sin 2\psi\cos\Delta & \sin 2\psi\sin\Delta \\ 0 & 0 & -\sin 2\psi\sin\Delta & \sin 2\psi\cos\Delta \end{pmatrix}. \quad (3)$$

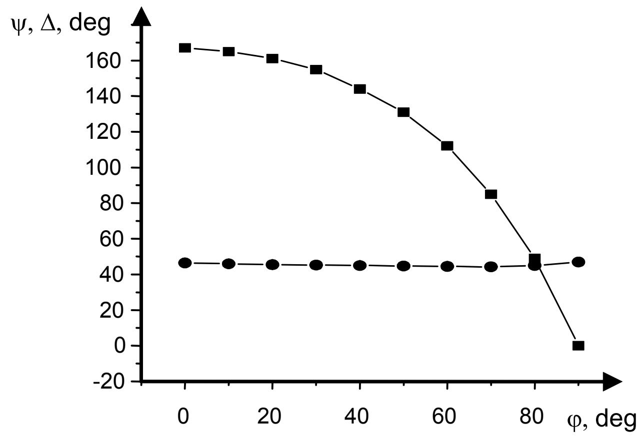

Fig. 1. Ellipsometric angles ψ (circles) and Δ (squares) for the air–mirror coating interface.

The ellipsometric angles Δ and ψ are plotted in Fig. 1 as functions of the incident angle for the air–mirror coating interface.

It can be seen that the reflection coefficients are equal for $\varphi \le 40°$, and at $\varphi = 70°$ $\rho_\perp/\rho_{II} = 0.948$, i.e., in the majority of cases we can take $2\psi \approx 90°$. If the normal to the tilted mirror lies in the plane of the electric vector of the laser beam or perpendicular to it, then linearly polarized light with $\boldsymbol{S}_0 = \{1,1,0,0\}$ or $\{1,-1,0,0\}$ is reflected without distortions. But if the normal to the mirror lies in a different plane, so that $\boldsymbol{E}$, i.e., the laser plane, has the matrix $\boldsymbol{S}_0 = \{1, a, b, 0\}$, then $\boldsymbol{S}_{01} = \{1, a, b\cos\Delta, -b\sin\Delta\}$ for the reflected beam, i.e., it is elliptical. The same holds for circular polarization: if $\boldsymbol{S}_0 = \{1,0,0,1\}$, then $\boldsymbol{S}_{01} = \{1, 0, \sin\Delta, \cos\Delta\}$.

The matrix of such an arbitrarily tilted mirror $\widehat{M}_{\mathrm{TM}}$ can be reduced to the polarization basis of the initial laser beam through the standard rotation matrix $\widehat{T}(2\theta)$, where θ is the angle between the projection of the mirror normal onto the plane perpendicular to the optical axis and the reference plane (as a rule, it is assigned as either the local vertical or the orientation of the polarization plane of the laser). Since $\widehat{M}_{\mathrm{TM}} = \widehat{T}(-2\theta)\widehat{M}\widehat{T}(2\theta)$, in our case

$$\widehat{M}_{\mathrm{TM}} = \begin{pmatrix} 1 & 0 & 0 & 0 \\ 0 & \cos^2 2\theta - \sin^2 2\theta & 2\cos 2\theta \sin 2\theta & 0 \\ 0 & -2\cos 2\theta \sin 2\theta \cos\Delta & (\cos^2 2\theta - \sin^2 2\theta)\cos\Delta & \sin\Delta \\ 0 & 2\cos 2\theta \sin 2\theta \sin\Delta & -(\cos^2 2\theta - \sin^2 2\theta)\sin\Delta & \cos\Delta \end{pmatrix}. \quad (4)$$

In the simplest cases θ = 0° and θ = 90° the matrices are equal

$$\widehat{M}_{\mathrm{TM}} = \begin{pmatrix} 1 & 0 & 0 & 0 \\ 0 & 1 & 0 & 0 \\ 0 & 0 & \cos\Delta & \sin\Delta \\ 0 & 0 & -\sin\Delta & \cos\Delta \end{pmatrix}. \quad (5)$$

In the case θ = 45° (a flat mirror tilted by 45° about one of its axes), the matrix

$$\widehat{M}_{\mathrm{TM}} = \begin{pmatrix} 1 & 0 & 0 & 0 \\ 0 & -1 & 0 & 0 \\ 0 & 0 & -\cos\Delta & \sin\Delta \\ 0 & 0 & \sin\Delta & \cos\Delta \end{pmatrix}. \tag{6}$$

Linear polarization is transformed into linear polarization, but with the polarization plane rotated by 90° since $\boldsymbol{S}_{01} = \{1, -1, 0, 0\}$. In the presence of several mirrors, say three, their total reflection matrix is given by $\widehat{M}_{\mathrm{TM}} = \widehat{M}_{\mathrm{TM1}} \cdot \widehat{M}_{\mathrm{TM2}} \cdot \widehat{M}_{\mathrm{TM3}}$.

In order to determine the actual return signal from the recorded return signal $\boldsymbol{S}$, that is, the signal arriving from the atmosphere or water onto the mirror and from there into the receiver (i.e., to solve the inverse problem), it is necessary to know the inverse matrix to $\widehat{M}_{\mathrm{TM}}$ since $\boldsymbol{S} = \widehat{M}_{\mathrm{TM}}^{-1} \boldsymbol{S}^1$. For matrix (4) the inverse matrix is

$$\frac{1}{m_{22}^2 + m_{23}^2} \begin{pmatrix} m_{22}^2 + m_{23}^2 & 0 & 0 & 0 \\ 0 & 0 & m_{32} & m_{42} \\ 0 & 0 & m_{33} & m_{43} \\ 0 & m_{22} \cdot m_{23} \cdot m_{34} \cdot m_{44} & (m_{22}^2 + m_{23}^2) \cdot m_{34} & (m_{22}^2 + m_{23}^2) \cdot m_{44} \end{pmatrix}, \tag{7}$$

where m_{ij} are the elements of mirror matrix (4). For the above considered simple cases, the inverse matrices are as follows:

$$\widehat{M}_{\mathrm{TM}}^{-1} = \begin{pmatrix} 1 & 0 & 0 & 0 \\ 0 & 1 & 0 & 0 \\ 0 & 0 & \cos\Delta & -\sin\Delta \\ 0 & 0 & \sin\Delta & \cos\Delta \end{pmatrix} \tag{8}$$

for the mirror tilted by 0° or 90° and

$$\widehat{M}_{\mathrm{TM}}^{-1} = \begin{pmatrix} 1 & 0 & 0 & 0 \\ 0 & -1 & 0 & 0 \\ 0 & 0 & -\cos\Delta & \sin\Delta \\ 0 & 0 & \sin\Delta & \cos\Delta \end{pmatrix} \tag{9}$$

for the mirror tilted by 45°, i.e., matrix (6) in this case is its own inverse.

In our lidar experiments [6] in water pools, we used two mirrors mounted symmetrically one above the other and tilted by 45° with respect to each other. This setup imitated the aviation scheme of laser sensing fairly closely. The laser beam passed horizontally above the water, was reflected from the first mirror, entered the water and was reflected by the second mirror and then passed through the water, again horizontally. In this case the matrix of the compound reflector, being the product of two ordinary matrices (6), becomes unitary and diagonal, which can be considered as a helpful effect, substantially simplifying the signal processing.

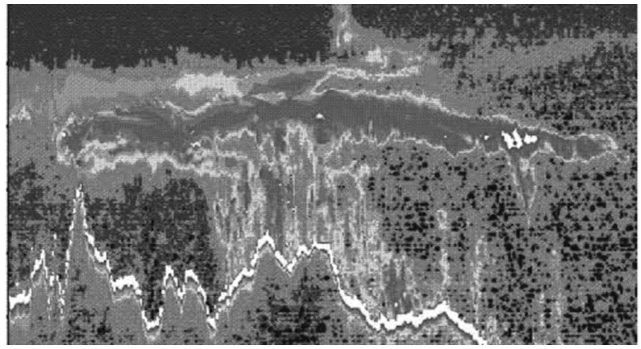

Fig. 2

In reality, the diagonal elements of the matrix are somewhat less than unity due to energy losses in the mirrors. Besides this, there is one more source of relatively weak distortions. In hydrooptical measurements, mirrors have been used having an internal coating for protection against the aggressive action of water. In front of the metallic layer there is a dielectric reflector (glass), for which the above matrices are unsuitable. However, the reflectivity of silver or aluminum is 25 times higher than the Fresnel reflection from the glass surface and its contribution to the matrix. In addition, for a mirror situated in water the refractive index of glass relative to water is close to unity, i.e., here the role of the glass component is decreased even further. In any case, in such a symmetric two-mirror system the lidar can operate both with linear and with circular polarization.

The situation is somewhat different with a tilted single mirror having reflection matrix (6). In the case of operating with linear polarization the mirror will not distort the Stokes vector. If the sensing laser beam has circular polarization, then after reflection from the mirror it becomes elliptical and this needs to be taken into account.

3. LASER SENSING OF THE ATMOSPHERE

In this section we present results of laser sensing of the atmosphere using the Atmaril lidar mounted on board an AN-30 aircraft-laboratory. Figure 2 displays a two-dimensional intensity plot of the optical signal, proportional to the aerosol mass concentration, above the Norilsk mining-and-metallurgical district. The flight altitude was 1000 m (upper border of the plot). The lower border is ground level. The length of the flight track was 30 km, which corresponds to 1600 laser pulses. Black segments here correspond to high turbidity, gray segments correspond to a clean atmosphere. The white segments are zones where the photomultipliers and analog-to-digital converters were overloaded.

An aerosol cloud of thickness 100–150 m is clearly visible, toward which aerosol streams are rising from the ground below. The maximum aerosol pollution level reaches 100–300 μg/m^3.

4. LASER SENSING OF THE UPPER LAYER OF THE OCEAN

Hydrooptical investigations by airborne lidar have a quite lengthy prehistory. For example, many interesting data were obtained during sensing of Lake Baikal [12]. But the most extensive experiments were conducted by us over the seas around Northern Scotland [13]. Figure 3 displays a contour map of the region of interest. The straight lines are the flight paths of the aircraft carrying the airborne lidar, and the numbers alongside them are the serial numbers of the runs.

Here investigations were undertaken of the spatial distribution of the water transparency. An example is given in Fig. 4. It was constructed from data of flight No. 4 toward the northwest from the Shetland Islands at a longitude of about 4° W. Longitude and flight time are plotted along the abscissa, and the length of this frame is 26 km. The laser pulse frequency was 1 Hz. The lower frame shows a horizontal profile of the attenuation coefficient of radiation for the

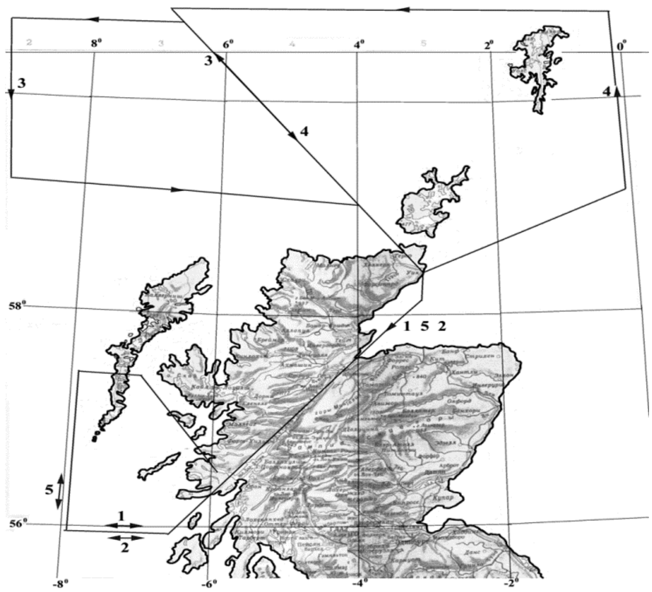

Fig. 3

wavelength 532 nm. The middle frame displays a color-coded plot of the depth distribution of the intensity of the depolarized component of the lidar return signal. The upper frame is the same for the polarized component. The vertical line between the lower and middle frames corresponds to the position of the local maximum of the attenuation coefficient and the maximum of the depolarization signal. Such a coincidence is not noted for the polarized component. In accordance with the canonical laws of light scattering this means that the strongly turbid segment of the lower frame is formed from nonspherical particles. Most likely, these are marine bio-organics. Many such segments with enhanced depolarization were observed during the course of the five flights that made up this mission. The dimensions of such inhomogeneities, i.e., "spots" of lowered or heightened transparency, varied from tens of meters to a few kilometers. A partial statistical analysis of these spots is provided in [13]. The standard deviation of the attenuation coefficient in such inhomogeneities reaches 40%.

Possibilities of the considered lidar in bathymetry are illustrated by Fig. 5, which displays depth profiles of the ocean bottom and the sea surface level above it for repeated overflights of the ridge of the Hebrides Islands. Straight line 5 to the west of Scotland in Fig. 3 corresponds to this region. The return signals were intentionally not corrected for the effect of taxiing of the aircraft (i.e., turns); therefore, the sea surface level appears uneven. The 20-meter depth scale is shown in the figure on the left. In these frames, bottom signals are observed to a depth of 20 m from the sea surface, and show up as a dark (i.e., high intensity of the received signal), almost horizontal line. Here it was also taken into account that the refractive index of water differs from that of air. Above the water surface, signals from the rocky islands are visible. It is interesting that in the right lower frame rocks appear that do not extend upward above the sea surface. Note also that at the time of our overflights of Lake Baikal, we were able to detect the bottom to depths of 35 m.

Figure 6 shows results of a shipborne experiment with the lidar mounted in a laboratory stateroom of the scientific vessel *Academician Keldysh*. These long-duration measurements were performed in the Sargasso Sea above the location of the wreck of the steamship *Titanic* within the compass of the Gulf Stream. That is, this was directed drift of the vessel. Water temperature is plotted along the abscissa, measured at different depths using shipborne equipment. Sensing depth is plotted along the ordinate. To avoid the need to solve the inverse problem of hydrooptical laser sensing with respect to the attenuation coefficient, the signals were reduced in several ranges of values of ADC code (i.e., bits) and represented as a gray scale and joined by isolines of equal intensity. The figure was constructed from 1500 laser pulses, where the signals of every 10 pulses were averaged to decrease the effect of sea surface waves. Spatially, this

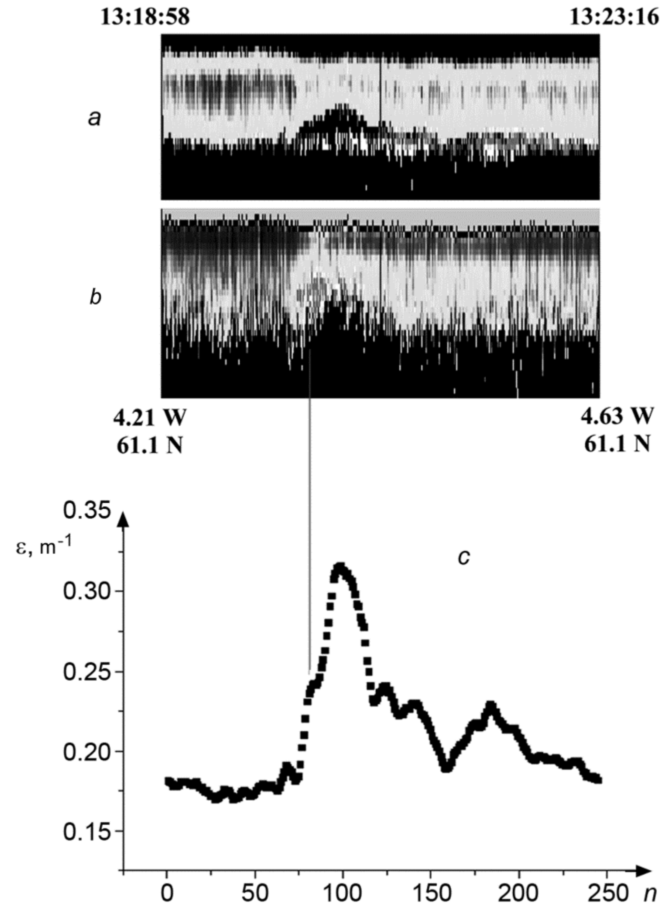

Fig. 4

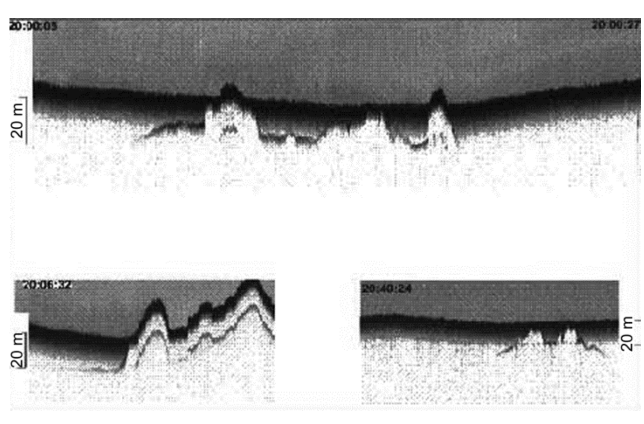

Fig. 5

corresponds to 4.5–6 km, taking into account the rate of flow. It is interesting to note that with lower temperature of the water mass the limiting depth of laser sensing also decreases. In passing, there is a quite logical explanation for this from the standpoint of bio-optics: the lower the water temperature, the higher its bioproductivity and, consequently, its attenuation coefficient. What is more, the isolines are multiply ragged, which speaks of the presence of some internal structure in that local underwater part of the Gulf Stream.

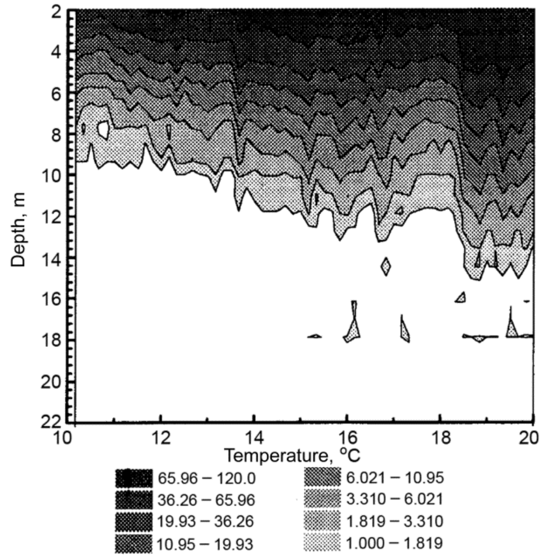

Fig. 6

CONCLUSIONS

It has been shown that the shipborne multipurpose automated lidar complex "Atmaril" allows one to detect local and spatially distributed sources of pollution in the atmosphere while realizing a quite rapid survey of large areas, allows mapping of the bottom depth in shallow water, and also allows one to estimate the horizontal and vertical structure of the upper layer of the ocean. This confirms the adequacy of the general principles and approaches to its functioning set forth in this paper. Lidar parameters are presented which have demonstrated their efficacy in practice in solving problems of laser sensing of the atmosphere and the upper layer of the ocean.

REFERENCES

1. J. H. Churnside, D. A. Demer, D. Griffith, *et al*., CalCOFI Rep., **50**, 118–122 (2009).
2. S. Yamagishi, K. Hitomi, H. Yamanouchi, and Y. Yamaguchi, Int. Oil Spill Conf., 929–933 (2001).
3. R. Barbini, F. Colao, R. Fantoni, *et al*., Proc. EARSeL-SIG-Workshop LIDAR, Dresden, 175–184 (2000).
4. R. Fantoni, R. Barbini, F. Colao, *et al*., EARSeL eProc., **3**, 43–53 (2004).
5. P. Chazette, J. Sanak, J.-C. Raut, and S. Berthier, Proc. of the 24th Int. Laser Radar Conf., Boulder, CO, NOAA-NASA, 95–98 (2008).
6. V. S. Shamanaev, I. E. Penner, M. M. Krekova, *et al*., Russ. Phys. J., **48**, No. 12, 1251–1256 (2005).
7. V. S. Shamanaev and G. P. Kokhanenko, Russ. Phys. J., **55**, No. 3, 269–272 (2013).
8. H. N. Antokhin, M. Yu. Arshinov, B. D. Belan, *et al*., J. Atm. Oceanic Techn., **29**, No. 1, 64–75 (2012).
9. A. P. Ivanov, Physical Principles of Hydrooptics [in Russian], Nauka i Tekhnika, Minsk (1975).
10. M. Born and E. Wolf, Principles of Optics, Pergamon Press, Oxford (1970).
11. R. M. A. Assam and N. M. Bashara, Ellipsometry and Polarized Light, Elsevier Science Publishing Co., New York (1987).
12. G. P. Kokhanenko, I. E. Penner, D. Ludbrook, *et al*., Opt. Atm. Okeana, **12**, No. 1, 39–45 (1999).
13. G. Kokhanenko, G. Ludbrook, I. Penner, and V. Shamanaev, Marine Geodesy, **24**, No. 4, 195–207 (2001).